



Chinese Pharmaceutical Association  
Institute of Materia Medica, Chinese Academy of Medical Sciences

Acta Pharmaceutica Sinica B

[www.elsevier.com/locate/apsb](http://www.elsevier.com/locate/apsb)  
[www.sciencedirect.com](http://www.sciencedirect.com)



ORIGINAL ARTICLE

# Engagement of $N^6$ -methyladenosine methylation of *Gng4* mRNA in astrocyte dysfunction regulated by CircHECW2



Ying Bai<sup>a</sup>, Di Chang<sup>b</sup>, Hui Ren<sup>a</sup>, Minzi Ju<sup>a</sup>, Yu Wang<sup>a</sup>, Biling Chen<sup>a</sup>, Han Li<sup>a</sup>, Xue Liu<sup>a</sup>, Daxing Li<sup>a</sup>, Xinchen Huo<sup>a</sup>, Xiaofei Guo<sup>a</sup>, Mengze Tong<sup>a</sup>, Ying Tan<sup>a</sup>, Honghong Yao<sup>a,c,d,e,\*</sup>, Bing Han<sup>a,\*</sup>

<sup>a</sup>Department of Pharmacology, Jiangsu Provincial Key Laboratory of Critical Care Medicine, School of Medicine, Southeast University, Nanjing 210009, China

<sup>b</sup>Department of Radiology, Zhongda Hospital, Jiangsu Key Laboratory of Molecular and Functional Imaging, Medical School of Southeast University, Nanjing 210009, China

<sup>c</sup>Co-Innovation Center of Neuroregeneration, Nantong University, Nantong 226001, China

<sup>d</sup>Institute of Life Sciences, Key Laboratory of Developmental Genes and Human Disease, Southeast University, Nanjing 210096, China

<sup>e</sup>Center for Global Health, School of Public Health, Nanjing Medical University, Nanjing 211166, China

Received 22 October 2023; received in revised form 8 December 2023; accepted 5 January 2024

## KEY WORDS

$N^6$ -Methyladenosine;  
Depression;  
circHECW2;  
Astrocyte;  
WTAP;  
Ubiquitination;  
GNG4;  
Dysfunction

**Abstract** The  $N^6$ -methyladenosine ( $m^6A$ ) modification is the most prevalent modification of eukaryotic mRNAs and plays a crucial role in various physiological processes by regulating the stability or function of target mRNAs. Accumulating evidence has suggested that  $m^6A$  methylation may be involved in the pathological process of major depressive disorder (MDD), a common neuropsychiatric disorder with an unclear aetiology. Here, we found that the levels of the circular RNA HECW2 (circHECW2) were significantly increased in the plasma of both MDD patients and the chronic unpredictable stress (CUS) mouse model. Notably, the downregulation of circHECW2 attenuated astrocyte dysfunction and depression-like behaviors induced by CUS. Furthermore, we demonstrated that the downregulation of circHECW2 increased the expression of the methylase WTAP, leading to an increase in *Gng4* expression via  $m^6A$  modifications. Our findings provide functional insight into the correlation between circHECW2 and  $m^6A$  methylation, suggesting that circHECW2 may represent a potential target for MDD treatment.

\*Corresponding authors.

E-mail addresses: [hanb@seu.edu.cn](mailto:hanb@seu.edu.cn) (Bing Han), [yaohh@seu.edu.cn](mailto:yaohh@seu.edu.cn) (Honghong Yao).

Peer review under the responsibility of Chinese Pharmaceutical Association and Institute of Materia Medica, Chinese Academy of Medical Sciences.

<https://doi.org/10.1016/j.apsb.2024.01.011>

2211-3835 © 2024 The Authors. Published by Elsevier B.V. on behalf of Chinese Pharmaceutical Association and Institute of Materia Medica, Chinese Academy of Medical Sciences. This is an open access article under the CC BY-NC-ND license (<http://creativecommons.org/licenses/by-nc-nd/4.0/>).

## 1. Introduction

Major depressive disorder (MDD) is a debilitating psychiatric disorder characterized by high rate of disability and suicide<sup>1–4</sup>. It is represented by significant psychosocial impairment, cognitive dysfunction, and impaired affect<sup>5,6</sup>. According to previous studies, with the complex mechanism, the outcomes of depression were the combined action of genes and environment<sup>7,8</sup>. Antidepressant medication, when used appropriately, has the potential to be helpful, and in some cases, it can even be life-saving. However, the outcomes are suboptimal given that approximately 50% of patients do not adequately respond<sup>9,10</sup>. Additionally, unpredictable therapeutic drugs may induce persistent depression and worse impairments. After remission of MDD patients, drugs for maintenance are suggested for 6 months to 1 year. However, after the withdrawal of drugs, there are no predictors for recurrence of MDD<sup>11</sup>. For these purposes, the exploration of biomarkers could be particularly informative for the diagnosis and prognosis of MDD, and deep research of the mechanisms helps investigate more potential targets. In summary, conducting intensive studies in this area has the potential to stimulate the development of new and innovative clinical approaches in the future.

N<sup>6</sup>-Methyladenosine (m<sup>6</sup>A) is a common mRNA modification and is present in physiological and pathological processes<sup>12,13</sup>. The dynamic regulation of m<sup>6</sup>A modification is mediated by specific enzymes, including writers, erasers, and readers. Writers, also known as methyltransferase, include Wilms tumor 1 associated protein (WTAP), methyltransferase-like 3 (METTL3), and methyltransferase-like 14 (METTL14), and are responsible for installing m<sup>6</sup>A modification. While erasers include several demethylases, such as AlkB homolog 5 (ALKBH5) and fat mass and obesity-associated protein (FTO)<sup>7</sup>. Readers, represented by YTH domain-containing proteins, recognize and bind to m<sup>6</sup>A-modified mRNAs, affecting various aspects of RNA metabolism and function<sup>14</sup>. Research has shown that methylation of m<sup>6</sup>A plays a broad and key role in biological processes in various organs or tissues<sup>15–18</sup>. Significantly, the previous study indicated that m<sup>6</sup>A in the central nervous system (CNS) showed a new perspective on the regulation of genes and that regulating the levels of m<sup>6</sup>A may be helpful for the pathophysiology of CNS disorders<sup>19</sup>. In addition, numerous proofs showed that ALKBH5 and FTO are associated with MDD<sup>7,20–22</sup>. Collectively, these studies point to the importance of m<sup>6</sup>A in MDD. However, the detailed mechanisms of the methyltransferase WTAP predicated in the physiological and pathological process of MDD remain to be further elucidated.

Circular RNAs (circRNAs), a type of non-coding RNAs, are produced by noncanonical back-splicing events and are highly expressed in CNS<sup>23,24</sup>. Many studies have indicated that they are involved in many pathological and physiological processes<sup>25–27</sup>. Due to their conservation, stability, and specificity of structure, circRNAs have important clinical potential in many aspects, as they could serve as potential biomarkers and direct effective treatment strategies for CNS diseases. Importantly, transcriptome analyses have shown abnormal expression of circRNAs in animal models and depressive patients<sup>7,28,29</sup>. Our earlier studies showed

that circRNAs may act as potential biomarkers and targets of therapy for depression<sup>7,26,28</sup>. Circular RNA HECW2 (circHECW2, mmu\_circ\_0000041) is a circular RNA with high conservation across mice and humans. It is derived from exons 11, 12, 13, and 14 of the HECW2 gene. Our previous research showed that circHECW2 levels were markedly increased in the hippocampus of LPS-treated mice<sup>30</sup>. However, the function of circHECW2 in depression remains unclear.

Astrocytes are the most abundant glial cells in the mammalian brain<sup>31</sup>, controlling multiple processes in the nervous system in healthy and diseased states<sup>32,33</sup>. They are versatile cells in the brain and participate in most functions as active players. Increasing evidence suggests that dysfunction of astrocytes plays a pivotal role in the development of depression<sup>34</sup>. For instance, astrocytes have been reported to mediate depression in the hippocampus through the release of ATP/adenosine<sup>35,36</sup> and to toxically depress synaptic transmission<sup>37</sup>. Moreover, astrocyte participation in depression has been found in many brain regions, suggesting that it is a general phenomenon in the brain<sup>38</sup>. More importantly, there has been a growing focus on an astrocyte-centric rather than a neuron-centric cause of MDD over the past two decades<sup>39</sup>.

In the study, we aimed to investigate the involvement of circHECW2-m<sup>6</sup>A methylation regulation in MDD. Specifically, we sought to elucidate the underlying molecular mechanisms, with a particular emphasis on the role of WTAP in mediating m<sup>6</sup>A modification of *Gng4* mRNA. Our findings provided compelling evidence that the downregulation of circHECW2 improved astrocyte function in depression by modulating m<sup>6</sup>A modifications of *Gng4* mRNA through WTAP. In summary, our results shed light on novel mechanisms that outline the interplay between circRNA and m<sup>6</sup>A methylation in MDD, underscoring the potential for treatments that directly target astrocytes in CNS diseases.

## 2. Materials and methods

### 2.1. Patients for clinical study

The protocol was approved by the Ethics Committee of Zhongda Hospital (approval ID: 2020ZDSYLL247-P01). Healthy controls (HCs) were recruited from the local community, and patients with MDD were recruited from the Department of Psychiatry, Zhongda Hospital. Written informed consent was obtained from all patients and HCs. The clinical characteristics of these subjects are listed in Tables 1–3.

### 2.2. Animal information

Adult male mice (C57BL/6J, 6–8 weeks old) were obtained from GemPharmatech Co., Ltd. Experiments of mice were performed in accordance with standard guidelines for the use of laboratory animals. All experiments were approved by the Institutional Animal Care and Use Committee of the Medical School, Southeast University.

**Table 1** Baseline participant characteristics.

Characteristic	HC group	MDD group	P value
	n = 52	n = 74	
Age (years)	38.73 ± 1.91	37.05 ± 1.55	0.490
Gender (Male) (%)	26.92% (14)	26.67% (19)	0.875
Education (years)	12.73 ± 0.76	11.25 ± 0.49	0.088
BMI (kg/m <sup>2</sup> )	24.09 ± 0.41	21.89 ± 0.36	0.000
Marital status (Single/Married/Divorced)	18/34/0	19/46/9	0.027
Family history (yes/no)	0/52	9/65	0.009
First episode (%)	NA	74.32% (55)	NA
On-set age (years)	NA	35.24 ± 1.55	NA

HC, healthy control; MDD, major depressive disorder; BMI, body mass index.

NA, not available.

All data are all presented as the mean ± SEM.

### 2.3. Human plasma collection and treatments

Plasma samples were collected from patients who did not receive drug therapy. Between 6:00 and 10:00 am, fasting venous blood (5 mL) was collected. Another 5 mL of blood was collected after the 2 weeks of MDD therapy. Firstly, the separation of plasma was collected at a speed of 1000×g for 15 min at 4 °C. The RNA was extracted from the plasma using Qiagen miRNeasy Serum/Plasma Kit (217184, Qiagen, USA) and was quantified using a

NanoDrop1000 (Thermo Fisher Scientific, USA). The prepared supernatant was transferred to RNase/DNase-free tubes and stored at −80 °C until further processing.

### 2.4. Chronic unpredictable stress (CUS) model

Animals were exposed to 1–2 randomly scheduled stressors per day for 4 weeks. The operations were as follows: (1) 24 h water deprivation, (2) 24 h food deprivation, (3) 24 h sawdust moistened

**Table 2** Depression information.

Characteristic	HC group	MDD group	P
	n = 52	n = 74	
HAMD-24	1.48 ± 0.19	28.68 ± 0.80	0.000
HAMD-Anxiety/somatization	0.51 ± 0.10	6.55 ± 0.25	0.000
HAMD-Weight	0.04 ± 0.03	0.78 ± 0.10	0.000
HAMD-Cognitive impairment	0.11 ± 0.04	4.23 ± 0.28	0.000
HAMD-Diurnal variation	0.00 ± 0.00	0.55 ± 0.08	0.000
HAMD-Retardation	0.15 ± 0.06	6.89 ± 0.21	0.000
HAMD-Sleep disturbance	0.48 ± 0.10	4.08 ± 0.21	0.000
HAMD-Feelings of despair	0.08 ± 0.04	4.55 ± 0.23	0.000
PHQ-9	2.19 ± 0.32	17.89 ± 0.63	0.000
MADRS	1.10 ± 0.21	27.54 ± 0.96	0.000
TEPS	80.90 ± 2.04	57.87 ± 2.49	0.000
TEPS-Anticipatory pleasure	43.92 ± 1.10	27.24 ± 1.13	0.000
TEPS-Consummatory pleasure	36.98 ± 1.05	30.64 ± 1.74	0.006
SHAPS	20.58 ± 0.85	36.82 ± 0.93	0.000
HAMA	1.69 ± 0.23	19.66 ± 0.96	0.000
HAMA-Physical anxiety	0.58 ± 0.13	7.49 ± 0.55	0.000
HAMA-Psychological anxiety	1.12 ± 0.18	12.18 ± 0.51	0.000
GAD-7	1.69 ± 0.38	13.64 ± 0.60	0.000

HC, healthy control; MDD, major depressive disorder; HAMD-24, 24-item Hamilton Depression Scale; HAMD-Anxiety/Somatization, Hamilton Depression Scale-Anxiety/Somatization factor; HAMD-Weight, Hamilton Depression Scale-Loss of weight factor; HAMD-Diurnal variation, Hamilton Depression Scale-Diurnal variation factor; HAMD-Cognitive impairment, Hamilton Depression Scale-Cognitive impairment factor; HAMD-Retardation, Hamilton Depression Scale-Retardation factor; HAMD-Sleep disturbance, Hamilton Depression Scale-Sleep disturbance factor; HAMD-Feelings of despair, Hamilton Depression Scale-Feelings of despair factor; PHQ-9, 9-items Patient Health Questionnaire; MADRS, Montgomery Asberg Depression Rating Scale; TEPS, Temporal Experience of Pleasure Scale; TEPS-Anticipatory pleasure, Temporal Experience of Pleasure Scale-Anticipatory pleasure; TEPS-Consummatory pleasure, Temporal Experience of Pleasure Scale-Consummatory pleasure; SHAPS, Snaith-Hamilton Pleasure Scale; HAMA, Hamilton Anxiety Scale; HAMA-Physical anxiety, Hamilton Anxiety Scale-Physical anxiety factor; HAMA-Psychological anxiety, Hamilton Anxiety Scale-Psychological anxiety factor; GAD-7, 7-item generalized anxiety disorder.

All data are all presented as the mean ± SEM.

**Table 3** Social psychological information.

Characteristic	HC	Depression	<i>P</i>
	<i>n</i> = 52	<i>n</i> = 74	
CTQ-T	32.54 ± 0.71	43.97 ± 1.73	0.000
CTQ-EA	5.75 ± 0.13	8.49 ± 0.58	0.000
CTQ-PA	5.11 ± 0.04	7.23 ± 0.45	0.000
CTQ-SA	5.08 ± 0.05	5.77 ± 0.21	0.006
CTQ-EN	9.00 ± 0.46	13.68 ± 0.61	0.000
CTQ-PN	7.60 ± 0.31	8.81 ± 0.37	0.020

HC, healthy control; MDD, major depressive disorder; CTQ, Childhood Trauma Questionnaire; CTQ-EA, Childhood Trauma Questionnaire-Emotional Abuse; CTQ-PA, Childhood Trauma Questionnaire-Physical Abuse; CTQ-SA, Childhood Trauma Questionnaire-Sexual Abuse; CTQ-EN, Childhood Trauma Questionnaire-Emotional Neglect; CTQ-PN, Childhood Trauma Questionnaire-Physical Neglect.

All data are all presented as the mean ± SEM.

with water, (4) 24 h absence of sawdust in the cage, (5) overnight illumination, (6) tail nipping, (7) 5 min forced swimming, (8) 3 h 45° cage-tilt, and (9) 6 h physical restraint.

## 2.5. Quantitative real-time PCR

According to earlier researches<sup>25,40</sup>, RNA was obtained by TRIzol reagent (15596026, Invitrogen, USA) and reversed by a HiScript Q RT SuperMix for qPCR Kit (R123-01, Vazyme, China). Then, it was quantified by SYBR Green Real-time PCR Master Mix (Q141-02, Vazyme, China). Cycle threshold was detected by the StepOne™ Real-Time PCR instrument (StepOne™ 4376357, applied biosystems®). All samples were run in duplicate. The information of primers is listed in Table 4.

## 2.6. Microinjection of the *shRNA-circHECW2* lentivirus

All mice were weighed before experiments and randomly assigned to different groups. C57BL/6J male mice were microinjected bilaterally with either the *shRNA-circControl-GFP* lentivirus or *shRNA-circHECW2-GFP* lentivirus (Hanbio, Shanghai, China) into the hippocampus using the following microinjection

coordinates: 2.06 mm behind the bregma and ±1.5 mm lateral from the sagittal midline at a depth of 2 mm from the skull surface.

## 2.7. Behavioural tests

Between 9:00 and 17:00, tests were performed in a sound-attenuated environment and were evaluated by the same researcher. Before the behavioral tests, animals were adjusted to the environment for at least 3 h. The results were investigated by the Plexon research solution system (Plexon Inc., Dallas, USA) by an experimenter who was blinded to the tested groups. The tests contained sucrose preference test (SPT), forced swim test (FST), and tail suspension test (TST).

### 2.7.1. SPT

According to early methods<sup>41</sup>, the SPT contains 3 steps. In step 1 (habituation), the sucrose solution (1%) was used to habituate animals for 3 days. In step 2 (sucrose preference at baseline), the researcher transferred one mouse to one cage and exposed to both sucrose solution and water at baseline for 24 h. In step 3 (sucrose preference at testing), two bottles were used for this step. One was filled with water, the other was filled with solution of sucrose (1%). These drinking options were performed for 24 h. The intake of sucrose solution and water were analyzed by subtracting the final weight of the bottles after 24 h of exposure from their initial weight.

### 2.7.2. FST

Animals were placed into a cylinder filled with water (15 cm) individually. After vigorous activity (2 min), mice acquired a posture of immobile. The immobility duration was recorded during the last 4 min of the 6 min.

### 2.7.3. TST

Animals were hung 50 cm above the ground by gummed tape placed 1 cm from the tip of the tail of mouse in the apparatus case. The 6-min test was recorded. First 2 min-the habituation period. Last 4 min-the duration of immobility (hanging passively without body movement).

## 2.8. Flow cytometry and cell sorting

Isolated brain cells were prepared from C57BL/6J mice. Tissue was digested by papain at 37 °C for 1 h (2 mg/mL, LS003119, Worthington, USA) in DMEM medium. Dispersed cells were filtrated with a nylon mesh (70 µm). The cells were resuspended in Percoll density gradient (30%, 17-0891-09, GE Healthcare, USA) and centrifuged (900×*g*) at 25 °C for 25 min. Next, the cells in the bottom were collected. After washing in PBS containing 2% FBS, the cells were blocked with FcR Blocking Reagent (130-092-575, Miltenyi Biotec). Astrocytes, microglial cells, neurons, and endothelial cells were marked by flow cytometry<sup>42–45</sup>. Cells were stained with PE anti-mouse ACSA-2 (130-116-244, Miltenyi Biotec, Germany), FITC anti-mouse/human CD11b antibody (101205, BioLegend, USA), PerCp-cy5.5 anti-mouse CD45 antibody (561869, BD Pharmingen, USA), APC anti-mouse NCAM-1/CD56 allophycocyanin MAb (FAB7820A-100, R&D, USA), and Brilliant Violet 605™ anti-mouse CD31 (102427, BioLegend, USA). After staining, the samples were sorted by FACS Aria II SORP (BD Biosciences, USA), and the data were analyzed using FlowJo\_V10 (FlowJo). Samples were gated for ACSA-2<sup>+</sup>

**Table 4** Information of PCR primers.

Oligonucleotide sequences 5'–3'	
circHECW2 (human)-F	CCCACCACTTGAACGCTAC
circHECW2 (human)-R	GGCTGTCAATGCGTGCCT
circHECW2 (mouse)-Forward	AACAGGGACCTCGTGGGATT
circHECW2 (mouse)-Reverse	GGCTGTCAATCCGTGCCTC
<i>Wtap</i> (mouse)-Forward	TAGACCCAGCGATCAACTTGT
<i>Wtap</i> (mouse)-Reverse	CCTGTTTGGCTATCAGGCGTA
<i>Gng4</i> (mouse)-Forward	GGCATGTCTAATAACAGCACCA
<i>Gng4</i> (mouse)-Reverse	CACTGGGATGATGAGGGGG
<i>GNG4</i> (human)-Forward	ACAGCACCCTAGCATCTCC
<i>GNG4</i> (human)-Reverse	GGCACTGGAATGATGAGAGG
<i>GAPDH</i> (human)-Forward	ACCATCTTCCAGGAGCGA
<i>GAPDH</i> (human)-Reverse	GGGCAGAGATGATGACCCTTT
<i>Gapdh</i> (mouse)-Forward	AGGTCGGTGTGAACGGATTTG
<i>Gapdh</i> (mouse)-Reverse	TGTAGACCATGTAGTTGAGGTCA

(astrocytes), ACSA-2<sup>-</sup>CD11b<sup>+</sup>CD45<sup>dim</sup> (microglial cells), NCAM-1/CD56<sup>+</sup> (neurons), and CD31<sup>+</sup> (endothelial cells). The RNeasy<sup>®</sup>-Micro Kit (74004, QIAGEN, Germany) was used for RNA extraction.

### 2.9. Western blot (WB)

Proteins were collected by lysate buffer (P0013B, Beyotime, China). Samples separated on sodium dodecyl sulfate-polyacrylamide gel electrophoresis (SDS-PAGE). Then, proteins were transferred onto polyvinylidene fluoride (PVDF) membranes<sup>46</sup>. The PVDF membranes were blocked with nonfat milk (5%) and probed with GFAP (60190-1-Ig, Proteintech, China), GNG4 (13780-1-AP, Proteintech, China), WTAP (60188-1-Ig, Proteintech, China), and GAPDH (60004-1-Ig, Proteintech, China) overnight at 4 °C. Then, they were incubated with HRP-conjugated affinipure goat anti-mouse IgG and anti-rabbit IgG (SA00001-1, SA00001-2, Proteintech, China). Results were detected by Tanon 5200.

### 2.10. Immunofluorescence (IF)

In our earlier studies<sup>47</sup>, tissue sections of 30 μm were prepared with a cryostat. The sections were incubated with H<sub>2</sub>O<sub>2</sub> for 10 min, incubated with 0.3% Triton X-100 in phosphate-buffered saline (PBS; 137 mmol/L NaCl, 2.7 mmol/L KCl, 10 mmol/L Na<sub>2</sub>HPO<sub>4</sub>, 2 mmol/L KH<sub>2</sub>PO<sub>4</sub>) for 15 min, and then blocked with 10% normal goat serum (NGS) in 0.3% Triton X-100 for 1 h at room temperature. Next, the sections were incubated with the anti-GFAP antibody (G3893, Sigma–Aldrich, USA) overnight. On the following day, the sections were washed, and incubated with Alexa Fluor 594 goat anti-rabbit IgG (A-11037, Thermo Fisher Scientific, USA) in PBS for 1 h at room temperature.

### 2.11. Primary mouse astrocyte cultures

P1 to P2 postnatal C57BL/6J WT mice were used to get the cells. The mice's brains were dissociated mechanically and used gauze to remove large blood vessels and membranes. Next, the dissected brains were digested with trypsin–EDTA (25200056, Gibco, USA). After digestion, the cells were plated on cell culture flasks which were precoated by poly-L-lysine. Then, the cells were incubated in CO<sub>2</sub> (5%) at 37 °C.

### 2.12. Measurement of total m<sup>6</sup>A

The modification level of total m<sup>6</sup>A was detected in picked up from the hippocampus of mice (200 ng RNA). The m<sup>6</sup>A levels were detected by the m<sup>6</sup>A RNA methylation quantification kit (P-9005, Epigentek, USA) according to the manufacturer's instructions. In brief, 200 ng of RNA was immobilized on strip wells employing RNA high-binding solution. The m<sup>6</sup>A modification was amplified and identified using specific capture and detection antibodies. Subsequently, the m<sup>6</sup>A signal was intensified and quantified calorimetrically by measuring absorbance at 450 nm in a microplate spectrophotometer.

### 2.13. RNA immunoprecipitation (RIP)

The hippocampus was ground in ice-cold PBS by a glass homogenizer until a cell suspension was obtained. The suspension was centrifuged at 1500 rpm, 5 min, 4 °C. The pellet of cells was

resuspended with an equal volume of complete RIP lysis buffer. RNA immunoprecipitation was performed with a Magna RIPTM RNA-binding protein immunoprecipitation kit (17–700 for the Magna RIP kit, 17–701 for the EZ-magna RIP kit, and 17–704 for the Magna RIP quad, Millipore, USA).

### 2.14. Luciferase assays

In the 3' UTR fragment of *Gng4*, there are five possible m<sup>6</sup>A modification sites, predicted by the "RRACH" motif (R = A/G, H = A/C/T) from the MeRIP-analysis. We generated a mutant fragment by replacing "A" with "T" in all the five possible m<sup>6</sup>A modification sites. Primary mouse astrocytes were transfected with pMIR-REPRORT luciferase vector with wildtype or mutated *Gng4* (RiboBio, China) for 24 h. According to the manufacturer's protocol (E2920, Promega, USA), reporter assays were experimented and analyzed.

#### (1) Wild-type m<sup>6</sup>A sites (*Gng4* 3' UTR)

GCTCCCATGTAGAGGCACACCTCCCACAACACCCCAT  
CTCTGTCCAACCAATCATGATCTGGGCTCATCTTGTTTTA  
TCATATTTCCCTTCATAGCACTGTTTCTCTTCTTTTTTTT  
TTCTTTTTTCTTATTCCATCCACAGAGAAAACAGACATT  
TTTATAGCCAAAAAACAAATGTGCCATATAAAAGTGTAG  
ACTTAAAGGTCTACAGTTTTTAAACATTCCCAACCATAA  
ATATATCCAGTTAATAAATTTCAAGTGGGTAATTCA.

#### (2) Mutant m<sup>6</sup>A sites (*Gng4* 3' UTR)

GCTCCCATGTAGAGGCACACCTCCCACAACACCCCAT  
CTCTGTCCAACCAATCATGATCTGGGCTCATCTTGTTTTAT  
CATATTTCCCTTCATAGCACTGTTTCTCTTCTTTTTTTTTT  
CTTTTTTCTTATTCCATCCACAGAGAAATCAGTCAATTTT  
ATAGCCAAAAATCAAATGTGCCATATAAAAGTGTAGTC  
AAAGGTCTACAGTTTTTAATCATTCCCAACCATAAATATAT  
CCAGTTAATAAATTTCAAGTGGGTAATTCA.

### 2.15. MR imaging data acquisition and functional data processing

MR imaging data were acquired using a 3.0 T MRI (Siemens MAGNETOM Trio, Erlangen, Germany) with a standard head coil at the Radiology Department of Zhongda Hospital. Subjects were instructed to stay still, remain awake, and avoid thinking of anything during the scan. The whole-brain fMRI dataset was taken based on BOLD signals. Images were acquired axially using a gradient echo-planar imaging (EPI) sequence and parameters were as follows: 36 slices, volume = 240, repetition time (TR) = 2000 ms, echo time (TE) = 25 ms, section thickness = 4 mm, gap = 0 mm, field of view (FOV) = 240 mm × 240 mm, acquisition matrix = 64 × 64, flip angle (FA) = 90°, and acquisition time = 8 min and 6 s. We then used 3D MPRAGE sequence to acquire high-resolution (1 mm<sup>3</sup>) T1-weighted images (sections = 176, TR/TE = 1900/2.48 ms, inversion time = 900 ms, FA = 90, FOV = 256 mm × 256 mm, and acquisition matrix = 256 × 256). Data analysis was conducted based on statistical parametric mapping (SPM8; <http://www.fil.ion.ucl.ac.uk/spm>). The preprocessing steps were used as previously described<sup>48,49</sup>, and a ROI based analysis of the average grey matter volume of the thalamus was then performed after extracting the grey matter volume using the mask of the thalamus in the AAL (Automated Anatomical Labeling) atlas.

### 2.16. Statistics

Analyses were performed by GraphPad Prism 8.0. The mean of the groups was compared using a Student *t*-test (for 2 groups) and ANOVA, followed by Bonferroni post-tests (for >2 groups). *P* values of <0.05 indicate statistical significance.

## 3. Results

### 3.1. *CircHECW2* is upregulated in CUS mice and MDD patients

CircHECW2 was highly expressed in the brain compared with other tissues (Fig. 1A and B). Our previous study first demonstrated that circHECW2 levels were increased in the hippocampus of LPS-treated mice<sup>30</sup>. It is noteworthy that LPS- and CUS-induced models of depression are well-documented in studies relevant to depression<sup>50–53</sup>. Thus, to investigate the potential involvement of circHECW2 in depression, we isolated the hippocampus and collected plasma from CUS mice. We observed elevated levels of circHECW2 in both the hippocampus and plasma of these mice (Fig. 1C and D). Next, we examined the levels of circHECW2 in the plasma of MDD patients and healthy control individuals (HCs), found that circHECW2 levels were markedly increased in MDD patients (Fig. 1E). Notably, our analysis revealed a positive correlation between circHECW2 levels and the scores of the Hamilton Rating Scale for depression 24 items (HAM-D-24) (Fig. 1F), the scores of the Montgomery-Asberg Depression Rating Scale (MADRS) (Fig. 1G), the scores of the Hamilton Anxiety Scale (HAMA) (Fig. 1H), and other scores (Supporting Information Fig. S1A–S1X). Moreover, the receiver operating characteristic (ROC) curve analysis revealed that the area under the curve (AUC) for circHECW2 was significant at 0.815, with a sensitivity of 0.743 and a specificity of 0.731 (Fig. 1I). Additionally, through linear regression analysis, we uncovered that MDD patients with elevated circHECW2 expression levels and high scores on the childhood trauma questionnaire (CTQ) displayed more severe depression symptoms (Fig. 1J). To assess the predictive capacity of circHECW2 levels for MDD outcomes, we examined the changes in circHECW2 level two weeks after treatment in MDD patient plasma and found that the level of circHECW2 was decreased 2 weeks after treatment in MDD patient plasma (Fig. 1K). The ROC curve analysis was performed between admission and the 2 nd week after admission to calculate the predictive power of baseline circSCMH1 levels for outcome as the AUC was 0.782 (Fig. 1L).

### 3.2. The downregulation of *circHECW2* ameliorates the behaviors induced by CUS

To validate the function of circHECW2 in depression, the shRNA-circCon or shRNA-circHECW2 lentivirus was micro-injected into the mice hippocampus, and subsequently, behavioral experiments were carried out following the induction of CUS (Fig. 2A and B). After microinjection for 2 weeks, we examined the efficacy of the lentiviral transduction and found that the expression of circHECW2 was decreased in shRNA-circHECW2-injected mice (Fig. 2C). Behavioural tests including sucrose preference test (SPT), forced swim test (FST), and tail suspension test (TST) were employed to evaluate the effect of circHECW2. The sucrose preference of the CUS-treated mice was decreased, indicative of anhedonia. Encouragingly, this deficit was

significantly alleviated by the downregulation of circHECW2 expression (Fig. 2D). In both the FST and TST, the time of immobility was notably prolonged in the CUS mice, and these effects were markedly ameliorated in shRNA-circHECW2-injected mice (Fig. 2E and F).

### 3.3. Role of *circHECW2* on astrocyte dysfunction in CUS mice hippocampus

Subsequently, we investigated the cellular mechanism through which circHECW2 affects functional recovery after CUS. To further assess the cell types in which circHECW2 expression is upregulated, we detected the expression of circHECW2 in astrocytes, microglia, neurons, and endothelial cells from the CUS mice brain (Fig. 3A). The results revealed a significant upregulation of astrocyte-derived circHECW2 in CUS compared to microglia-, neuronal-, or endothelial cell-derived circHECW2 (Fig. 3B). Additionally, the fluorescence *in situ* hybridization staining indicated that circHECW2 was abundant in astrocytes (Fig. 3C). Furthermore, shRNA-circHECW2 treatment significantly mitigated the decrease in GFAP expression observed in CUS mice (Fig. 3D and E). Then, we detected the function of shRNA-circHECW2 on the astrocyte's morphology using GFAP and 3D reconstruction (Fig. 3F). Sholl analysis indicated that astrocyte dysfunction was induced by CUS, as evidenced by a reduction in branch numbers, length, and volume of astrocytes. Importantly, these deficits were markedly improved by shRNA-circHECW2 treatment (Fig. 3G–I). Taken together, these results suggest that the abnormal upregulation of circHECW2 in astrocytes may represent a critical molecular event in the progression of depression.

### 3.4. *circHECW2* inhibits m<sup>6</sup>A methylation by downregulating WTAP

Given the potential role of m<sup>6</sup>A methylation in MDD and the mutual regulation between circRNAs and m<sup>6</sup>A methylation<sup>7,19</sup>, we embarked on an investigation to determine whether circRNA's regulatory role in the pathological processes of depression, particularly in astrocyte-mediated mechanisms, involves m<sup>6</sup>A modifications. CUS led to a decrease in m<sup>6</sup>A levels in the hippocampus, an effect that was significantly mitigated by shRNA-circHECW2, indicating a regulation of circHECW2 on m<sup>6</sup>A methylation (Fig. 4A). We next measured the expression of m<sup>6</sup>A-modifying enzymes above in CUS mouse models both in mRNA and protein levels, found that only the protein level of WTAP was reduced in the hippocampus of CUS mice (Fig. 4B, Supporting Information Figs. S2 and S3A–S3D). Subsequently, we used mouse primary astrocytes transduced with shRNA-circHECW2 lentivirus or circHECW2-overexpressed plasmid for further investigations (Fig. 4C and D). The expression of WTAP was significantly increased in shRNA-circHECW2-treated cells (Fig. 4E), whereas the Western blot analysis indicated that circHECW2 did not alter the levels of METTL3, METTL14, FTO, and ALKBH5 (Supporting Information Fig. S4A–S4D), suggesting a specific association between circHECW2 and WTAP. To confirm these findings, primary astrocytes were transduced with the circHECW2 circHECW2-overexpressed plasmid and WTAP was significantly decreased in astrocytes (Fig. 4F). Next, pull-down assay was used to explore the interaction between circHECW2 and WTAP, and circHECW2 showed a stronger affinity to WTAP (Fig. 4G). Furthermore, *in vivo* experiments demonstrated that shRNA-circHECW2 significantly improved the decrease in

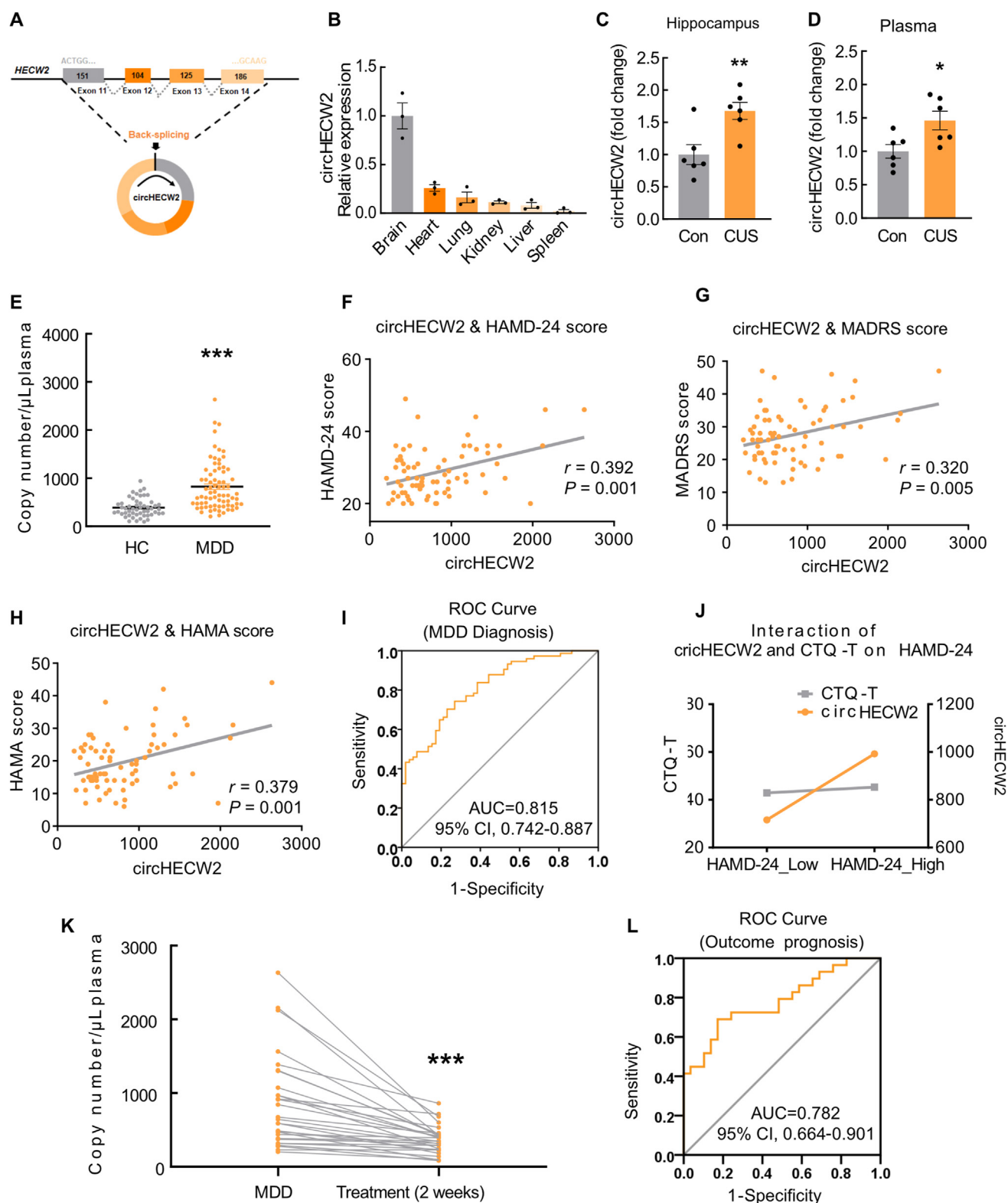


**Figure 1** CircHECW2 was upregulated in CUS mice and patients with MDD. (A) The exon composition of circHECW2. (B) The expression of circHECW2 in different organs of mice. (C) The levels of circHECW2 were increased in the hippocampal tissues of CUS mice compared with controls ( $n = 6$  mice/group). (D) The levels of circHECW2 were decreased in the plasma of CUS mice compared with controls ( $n = 6$  mice/group). (E) The expression of circHECW2 was increased in the plasma of MDD patients ( $n = 50$ ) compared with normal control individuals ( $n = 74$ ). (F–H) Correlations between circHECW2 expression and HAMD-24 (F), MADRS (G), and HAMA (H) scores using Pearson's correlation coefficient. (I) Receiver operating characteristic (ROC) curves were calculated using the baseline levels of circHECW2 based on the replication cohort as the training set for differentiating between patients with MDD and HCs. (J) The interactive effects of circHECW2 and CTQ-T on HAMD-24. (K) The levels of circHECW2 were decreased in the plasma of MDD patients after 2 weeks of treatment (\*\*\*). (L) ROC curves were calculated using the baseline levels of circHECW2 based on the replication cohort as the training set for differentiating between patients with MDD and HCs.

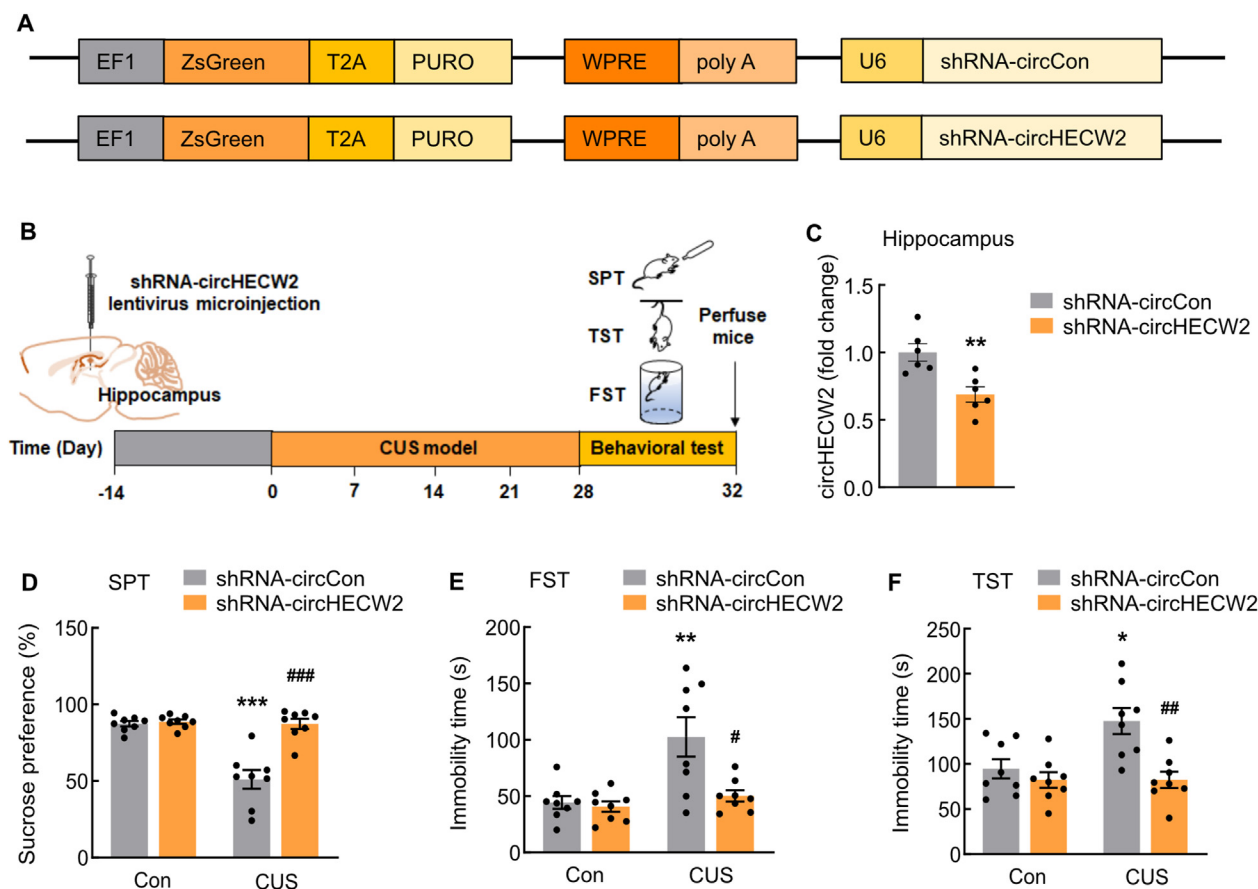


**Figure 2** Downregulation of circHECW2 ameliorated depressive-like behaviors induced by CUS. (A) Schematic of the lentivirus encoding circHECW2. (B) Timeline of the experimental procedure in the CUS-induced mouse model of depression. (C) CircHECW2 expression was measured by real-time PCR in the mouse hippocampus. (D–F) Effect of shRNA-circHECW2 lentivirus microinjection on depressive-like behaviors in CUS mice. Two weeks after the shRNA-circControl/shRNA-circHECW2 lentivirus microinjection, mice were exposed to a CUS or control ( $n = 8$  mice/group). SPT (D), FST (E), and TST (F) were measured after 4 weeks of CUS exposure. All data are presented as the mean  $\pm$  SEM. \* $P < 0.05$ , \*\* $P < 0.01$ , \*\*\* $P < 0.001$  versus shRNA-circControl, # $P < 0.05$ , ### $P < 0.01$ , #### $P < 0.001$  versus shRNA-circControl CUS.

WTAP expression induced by the CUS model (Fig. 4H). To explore why WTAP decreased after CUS, we employed immunoprecipitation to detect ubiquitination. The lysine 48-linked ubiquitination (Ub-K48) level of WTAP was significantly decreased by circHECW2 knockdown in the CUS model (Fig. 4I).

Next, we investigated the effect of circHECW2 and WTAP on the survival of astrocytes. Corticosterone was used to mimic the depression *in vitro*<sup>7</sup>. Astrocytes transduced with shRNA-circHECW2 showed an amelioration of the decreased viability induced by corticosterone (Fig. 4J). In contrast, knockdown the expression of WTAP significantly aggravated the decreased viability of astrocytes treated with corticosterone (Fig. 4K). Furthermore, WTAP siRNA decreased viability of astrocytes was ameliorated by shRNA-circHECW2, further indicating a close relationship between circHECW2 and WTAP (Fig. 4L).

Additionally, we constructed a brain astrocyte-specific AAV-GFAP-WATP knockdown (KD) virus. Three weeks after the microinjection of AAV-GFAP-WATP KD and shRNA-circHECW2 lentivirus in the hippocampus, the mice were subjected to CUS or control. Behavioral experiments including SPT, FST, and TST were examined after 4 weeks of CUS exposure. As shown in new Supporting Information Fig. S5A, the increased sucrose preference in shRNA-circHECW2 lentivirus-microinjected mice was abolished after astrocyte-specific WTAP knockdown. In both FST and TST, the immobility time was significantly reduced in shRNA-circHECW2 lentivirus-microinjected CUS mice compared with vector-control-microinjected CUS mice, and astrocyte-specific WTAP knockdown reversed these effects (Fig. S5B and S5C). These results demonstrated the causal role of WTAP in the downstream of circHECW2 in astrocytes of CUS mice.

scores on HAMD-24 scores in MDD patients using multivariate linear regression. MDD patients with high circHECW2 levels and CTQ scores showed more severe depression symptoms. (K) The temporal expression profiles of circHECW2 were detected by real-time PCR ( $n = 29$ ). (L) ROC curves were calculated based on the  $\Delta$  value (copy number/ $\mu$ L on the 2nd week minus copy number/ $\mu$ L on the first day) of circHECW2. All data are presented as the mean  $\pm$  SEM. \* $P < 0.05$ , \*\* $P < 0.01$ , \*\*\* $P < 0.001$  versus control.

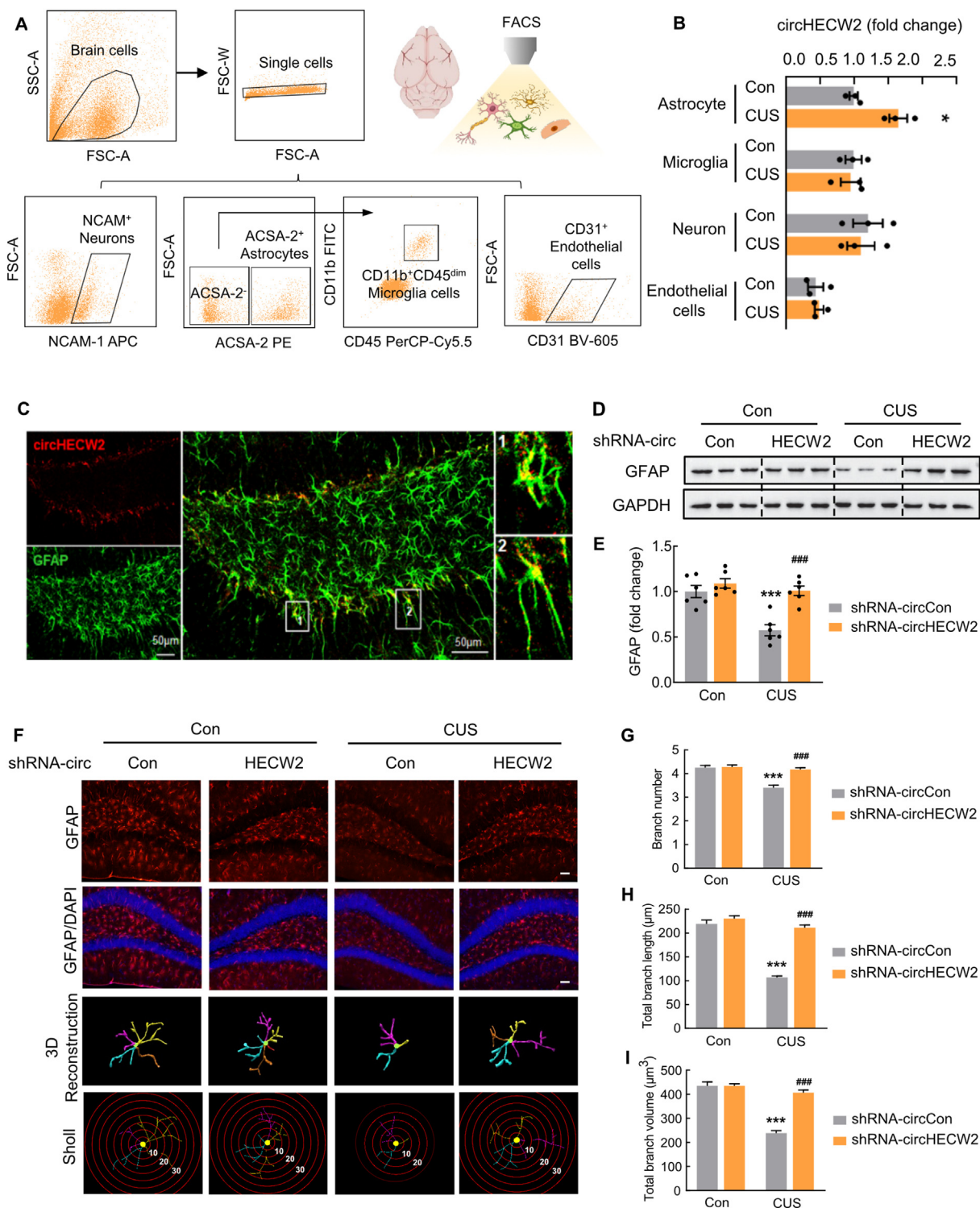


**Figure 3** Downregulation of circHECW2 attenuated astrocyte dysfunction in the CUS mouse hippocampus. (A) Schematic of astrocyte, microglia, neuron, and endothelial cell isolation from CUS and control groups. (B) Relative expression of circHECW2 in the sorted cells as determined by real-time PCR.  $n = 3$  samples for each group. (C) CircHECW2 accumulated in astrocytes of the hippocampus, which was detected by FISH analysis followed by immunohistochemistry using antibodies against GFAP. Scale bar: 50 μm. (D, E) Western blot analysis of GFAP expression in CUS mice model. Three representative immunoblots from 6 mice/group are presented. (F–I) Effect of circHECW2 on the astrocyte activation induced by CUS. Representative images of astrocyte immunostaining for GFAP in the mouse hippocampus, followed by 3D reconstruction and Sholl analysis (F), branch number (G), total branch length (H), and total branch volume (I). Scale bar: 50 μm. All data are presented as the mean ± SEM.  $n = 4$  mice/group, 40 cells/group. \* $P < 0.05$ , \*\*\* $P < 0.001$  versus the Control group; ### $P < 0.001$  versus the circControl-CUS group.

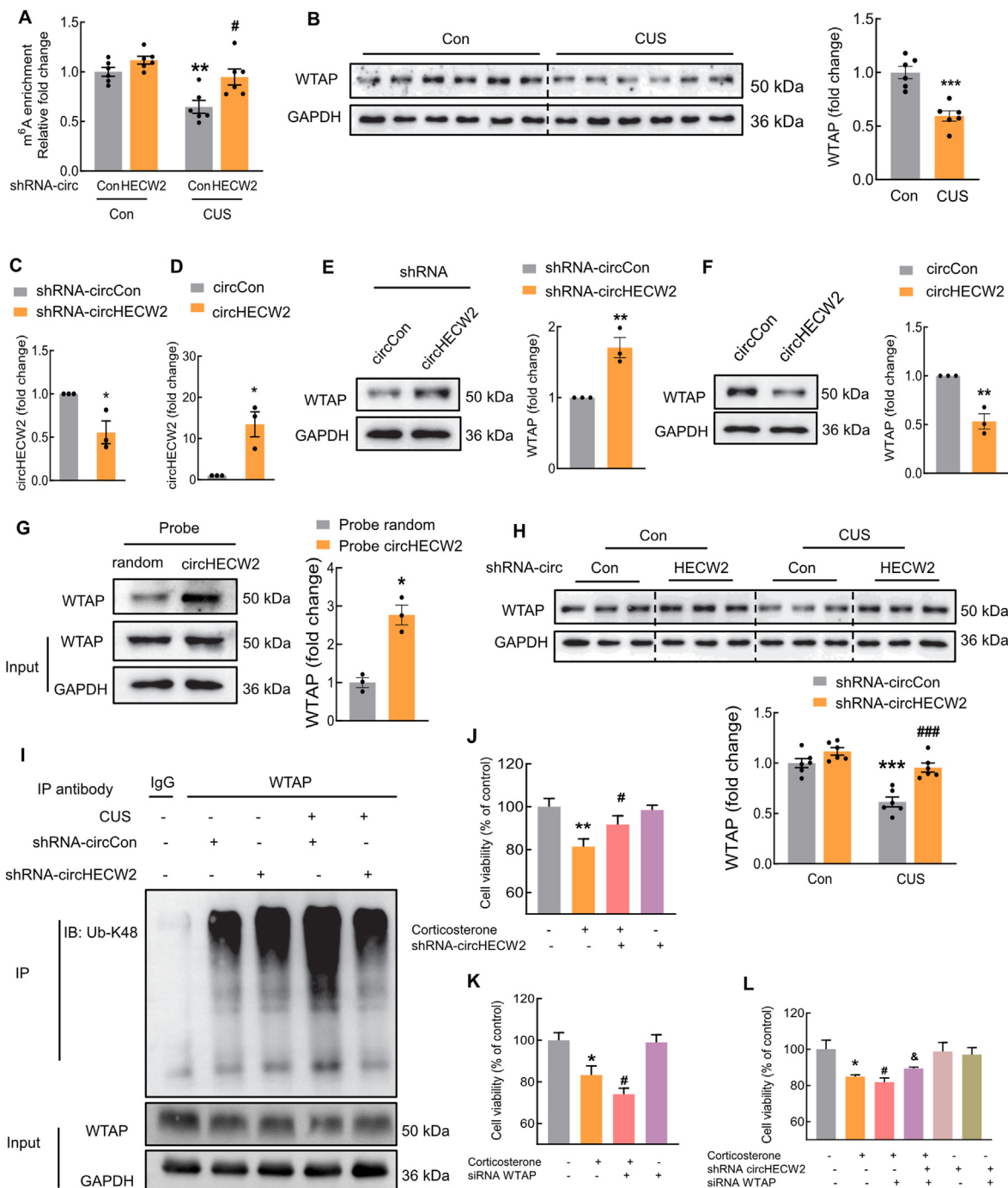


**Figure 4** CircHECW2 inhibited m<sup>6</sup>A methylation by downregulating WTAP. (A) Total RNA was extracted from the mouse hippocampus, and m<sup>6</sup>A levels were determined as a percentage of all adenosine residues in RNA.  $n = 6/\text{group}$ . (B) Western blot analysis showed that WTAP was decreased in the hippocampus of CUS mice compared with the control group.  $n = 6/\text{group}$ . (C) The level of circHECW2 was decreased in primary mouse astrocytes transduced with shRNA-circHECW2. (D) The level of circHECW2 was decreased in primary mouse astrocytes transduced with circHECW2. (E) Western blot analysis showed that WTAP was increased in astrocytes transduced with shRNA-circHECW2. (F) Western blot analysis showing that WTAP expression was decreased in primary mouse astrocytes transduced with circHECW2. (G) RNA pull-down assay was performed with a circHECW2 probe. (H) Western blot analysis showing WTAP expression in CUS mice. Three representative immunoblots from 6 mice/group are presented.  $*P < 0.05$ ,  $**P < 0.01$ ,  $***P < 0.001$  versus the shRNA-circControl Control group;  $\#P < 0.05$ ,  $###P < 0.001$  versus the shRNA-circControl CUS group. (I) Immunoprecipitation detected Ub-K48 modification of WTAP in the CUS mouse model. (J–L) Protective effect of shRNA-circHECW2 and WTAP siRNA on astrocyte loss induced by corticosterone. All data are presented as the mean  $\pm$  SEM.  $*P < 0.05$ ;  $**P < 0.01$  versus the control group;  $\#P < 0.05$  versus the corticosterone group;  $\&P < 0.05$  versus the corticosterone group with WTAP siRNA treatment.

### 3.5. WTAP regulates m<sup>6</sup>A modification of *Gng4* mRNA in depression

To seek the potential downstream molecule that participated in the CUS mouse, we posted a transcriptome-wide detection of m<sup>6</sup>A modification in the hippocampus of the CUS mouse in previous study<sup>7</sup>. As shown in Fig. 5A, the gene ontology biological processes (GO-BP) analysis showed that the downregulated genes were enriched in gene terms associated with the cellular process. The region of mRNA with altered m<sup>6</sup>A modification (downregulated genes) (Fig. 5B). Next, RNA-seq analysis was performed in the hippocampus of the CUS mouse model. We identified 288 genes that were differentially expressed in RNA-seq analysis (Cuffdiff adjusted *P*-value<0.05) (Fig. 5C, Supporting Information Table S1). Of particular interest, there were 19 overlapping transcripts between the two comparisons (Fig. 5D), suggesting that these genes may be the target genes involved in astrocyte dysfunction after CUS. Notably, these 19 overlapping transcripts were verified at the mRNA level. In the 4 upregulated transcripts, no gene was validated (Supporting Information Fig. S6A). Nevertheless, among the 15 downregulated transcripts, *Mfip*, *Eng*, *Gng4*, *Slc22a8*, and *Fxyd1* levels were in accordance with transcriptome sequencing (Fig. S6B). Additionally, *GNG4* was significantly decreased in the plasma of MDD patients (Supporting Information Fig. S7A–S7E). Additionally, there was a negative correlation between *GNG4* and the scores of the HAMD-Cognitive impairment (Supporting Information Fig. S8A–S8H). Based on these findings, *GNG4* emerged as a central focus in our study of MDD. Furthermore, we analyzed the pathway involving *GNG4* and its association with decreased m<sup>6</sup>A modification by Kyoto Encyclopedia of Genes and Genomes (KEGG) (Fig. 5E). Next, further results indicated that m<sup>6</sup>A modification was decreased in the peak region (chr13: 13825437–13825707) in the 3'-UTR of *Gng4* mRNA (Fig. 5F and G). We employed luciferase assays to compare the wild-type (WT) and mutant m<sup>6</sup>A sites with and without WTAP siRNA treatment. These assays demonstrated that the mutation prevented methylation and increased the stability of *Gng4* mRNA (Fig. 5H). As expected, overexpression of *Gng4* markedly ameliorated the declined viability of astrocytes treated with corticosterone (Fig. 5I).

### 3.6. CircHECW2 regulates m<sup>6</sup>A methylation of *Gng4* mRNA via WTAP

Furthermore, we examined the expression and function of *GNG4* in the CUS mouse model. The mRNA and protein levels of *Gng4* were significantly decreased in the hippocampus of CUS mice, which was consistent with the decreased m<sup>6</sup>A modification of *Gng4* (Fig. 6A and B). In addition, to understand the relationship between *Gng4* levels and the WTAP, WTAP siRNA was transfected in mouse primary astrocytes. The expression of *GNG4* and *Gng4* mRNA are all decreased (Fig. 6C). Moreover, the upregulation of circHECW2 led to reduced mRNA and protein levels of *Gng4* (Fig. 6D). Conversely, the downregulation of circHECW2 in astrocytes increased the mRNA and protein levels of *Gng4* (Fig. 6E). Co-transfection of WTAP siRNA and shRNA-circHECW2 indicated that WTAP siRNA decreased the *GNG4* level, which was markedly ameliorated by shRNA-circHECW2 (Fig. 6F). To validate these *in vitro* findings, Western blot analysis was performed to assess the levels of *GNG4* in shRNA-circHECW2-treated CUS mice. The results showed that

shRNA-circHECW2 treatment significantly mitigated the decrease in *GNG4* expression observed in CUS mice (Fig. 6G and H). We also constructed a brain astrocyte-specific AAV-GFAP-*Gng4* KD virus. Three weeks after the microinjection of AAV-GFAP-*Gng4* KD and shRNA-circHECW2 lentivirus into the hippocampus, the mice were exposed to CUS or kept in a control condition. The results of SPT, FSF, and TST revealed that astrocytic *Gng4* is involved in the regulation of circHECW2 in depression (Fig. 6I–K).

### 3.7. Hippocampus functional connectivity to the prefrontal cortex was positively correlated with *GNG4* in MDD patients

Finally, the seed-to-voxel analysis (hippocampal functional connectivity) was performed and showed hippocampus functional connectivity (FC) with prefrontal cortex (PFC) in MDD patients. As shown in Fig. 7A–C, the FC between the hippocampus and the prefrontal cortex was significantly reduced in MDD patients when compared to HCs. We next identified a noteworthy decrease in the resting-state functional connectivity (rsFC) between the hippocampus and the dorsolateral prefrontal cortex (Fig. 7D), whereas other brain regions, such as the visual cortex and inferior temporal lobe, exhibited no significant difference (Supporting Information Fig. S9). Moreover, we found a positive correlation between *GNG4* levels and rsFC, suggesting that *GNG4* may play a role in the cognitive brain function of individuals with MDD (Fig. 7E).

## 4. Discussion

Our study demonstrated that upregulation of circHECW2 led to the decrease in *Gng4* mRNA via WTAP-mediated m<sup>6</sup>A modification, and caused subsequent astrocyte dysfunction. Specifically, circHECW2 promoted the ubiquitin-mediated degradation of WTAP in the CUS mouse model, and the effect of *GNG4* on maintaining normal astrocyte functions is abolished when WTAP is downregulated in astrocytes. Therefore, the circHECW2/WTAP/*GNG4* axis regulates astrocyte dysfunction by decreasing *GNG4* stability via WTAP-mediated m<sup>6</sup>A modification, as depicted in Fig. 8. In conclusion, our findings indicate that circHECW2 holds promise as a therapeutic target for the treatment of depression. In addition, our study sheds light on the functional link between circHECW2 and m<sup>6</sup>A methylation, offering novel insights for the development of preventive strategies and effective treatments for MDD.

Our study represents an advance in the field, as it demonstrated that circHECW2 holds potential as a biomarker for both the diagnosis and prognosis of MDD. While the precise mechanisms governing the interaction between circHECW2 levels in the periphery and the brain during MDD are yet to be fully elucidated, the consistent dysregulation of circHECW2 levels in both the plasma and hippocampus suggests the intriguing possibility that circRNAs may actively cross the blood–brain barrier<sup>26</sup>. In patients with MDD, the expression of circHECW2 in plasma was found to be positively correlated with HAMD-24, which is a commonly used clinical tool for assessing depression severity. Additionally, circHECW2 exhibited positive correlations with MADRS and HAMA scores, further underscoring its potential as a diagnostic marker for MDD. Moreover, our study also revealed that there was an interactive effect between circHECW2 and childhood trauma events on the severity of anhedonic symptoms in MDD patients, emphasizing that the development of MDD is

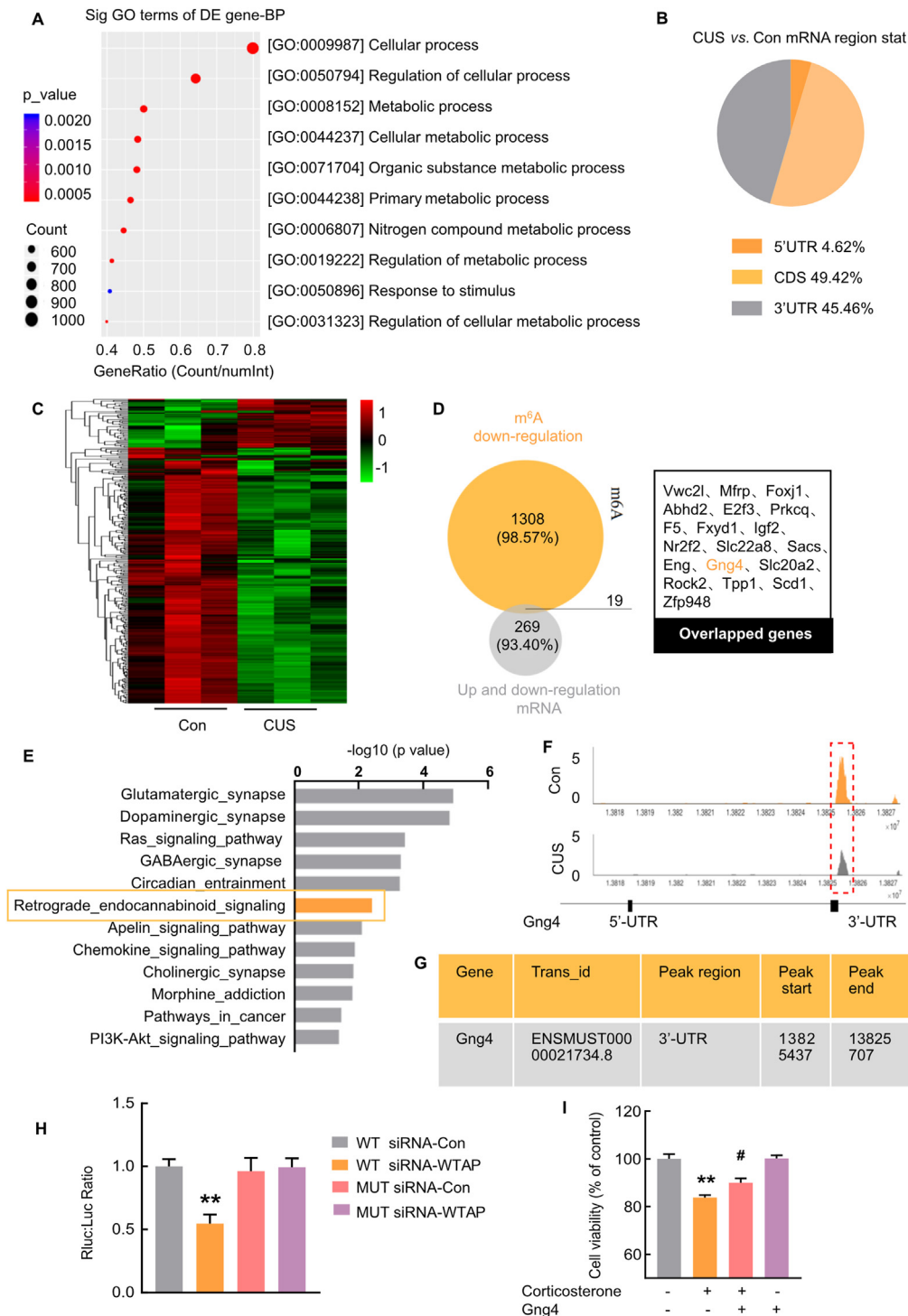


**Figure 5** WTAP regulated m<sup>6</sup>A modification of *Gng4* mRNA in the CUS mouse. (A) Gene ontology (GO) analysis was used for the analysis of the downregulation genes of m<sup>6</sup>A modification. The bar plot shows the top ten downregulated Enrichment Score values of the significant enrichment BP. (B) Pie chart depicting the fraction of m<sup>6</sup>A peaks. (C) The heatmap shows that clustering based on the differentially expressed genes allowed complete separation between Con and CUS groups. Gene expression levels were standardized and displayed as gradient colors from higher (red) to lower (green). (D) Venn diagram showed the overlap between genes with downregulation genes of m<sup>6</sup>A modification and genes that were differentially expressed in RNA-seq. (E) The significantly enriched depression-associated pathways of *Gng4*. (F) Abundant m<sup>6</sup>A in *Gng4* mRNA transcripts. m<sup>6</sup>A peaks in red rectangles have significantly reduced abundance (fold change > 1.5). (G) M<sup>6</sup>A peaks information of *Gng4*. (H) Luciferase assays were performed in astrocytes transfected with WT or mutant luciferase *Gng4* 3'-UTR reporters. (I) Protective effect of *Gng4* on astrocyte loss induced by corticosterone. All data are presented as the mean  $\pm$  SEM. \* $P$  < 0.05; \*\* $P$  < 0.01 versus the control group; # $P$  < 0.05 versus the corticosterone group.

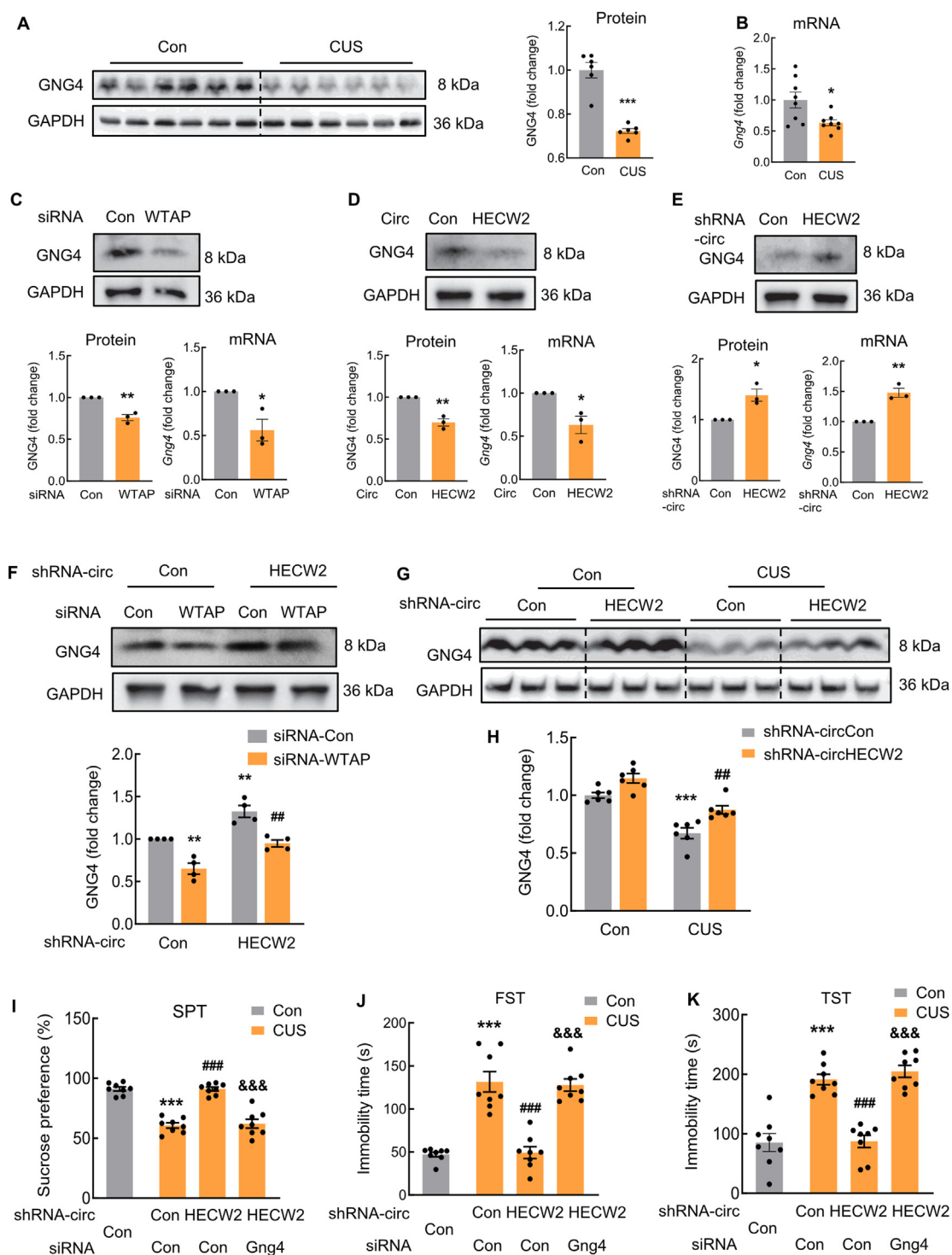


**Figure 6** CircHECW2 regulated m<sup>6</sup>A methylation of *Gng4* mRNA via WTAP. (A) Western blot analysis showed that GNG4 was decreased in the hippocampus of CUS mice compared with the control group.  $n = 6/\text{group}$ . (B) Real-time PCR showed that GNG4 was decreased in the hippocampus of CUS mice compared with the control group.  $n = 8/\text{group}$ . (C) The level of GNG4 and *Gng4* mRNA were decreased in primary mouse astrocytes transduced with WTAP siRNA. (D, E) The level of GNG4 and *Gng4* mRNA was decreased in primary mouse astrocytes transduced with circHECW2 (D) or shRNA-circHECW2 (E). (F) Western blot analysis showing the expression of GNG4 in primary mouse astrocytes co-transduced with WTAP siRNA and shRNA-circHECW2. (G, H) Western blot analysis of GNG4 expression in CUS mice model. (I–K) Effect of siRNA *Gng4* adeno-associated virus and shRNA-circHECW2 lentivirus microinjection on depressive-like behaviors in CUS mice. Three weeks after the virus microinjection, mice were exposed to a CUS or control ( $n = 8$  mice/group). SPT (I), FST (J), and TST (K) were measured after 4 weeks of CUS exposure. All data are presented as the mean  $\pm$  SEM. \* $P < 0.05$ , \*\* $P < 0.01$ , \*\*\* $P < 0.001$ , # $P < 0.05$ , ### $P < 0.01$ , #### $P < 0.001$ .

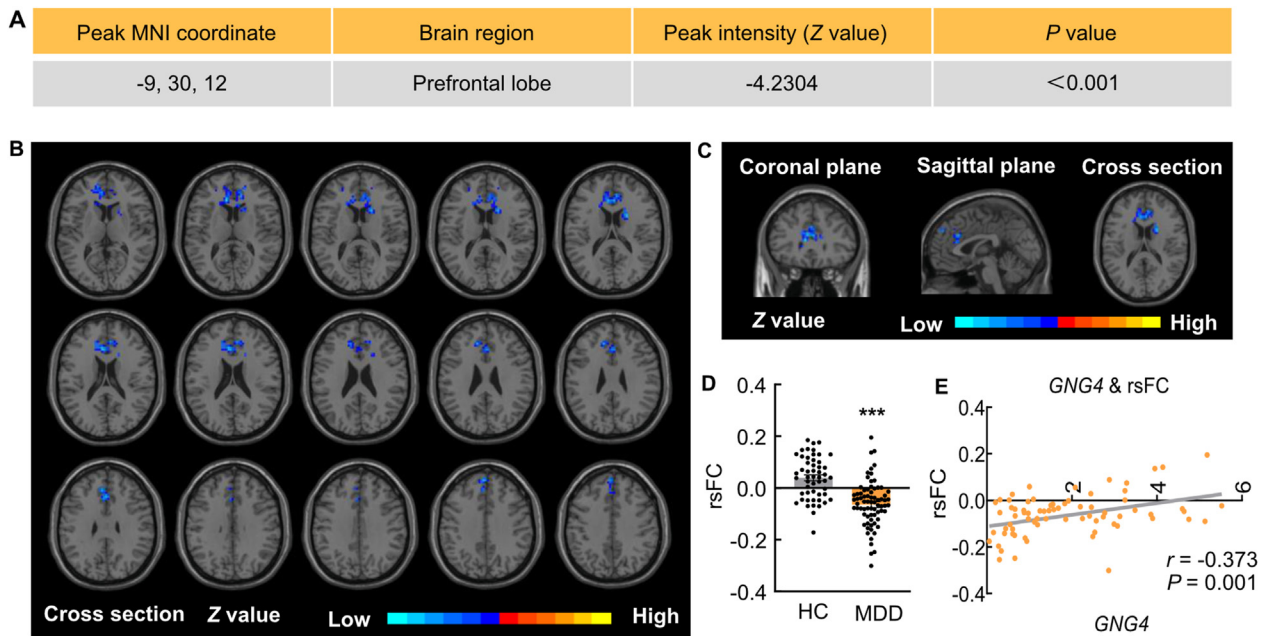


**Figure 7** Hippocampus FC with PFC was positively correlated with *GNG4* in MDD patients. (A–D) rsFC was decreased in the hippocampus FC with PFC of MDD patients compared with HCs. (E) Correlations between *GNG4* expression and rsFC using Pearson’s correlation coefficient. FC, functional connectivity; PFC, prefrontal cortex; MNI, Montreal Neurological Institute. All data are presented as the mean ± SEM. \*\*\* $P < 0.001$ .

influenced by a complex interplay of both biological and environmental factors. Furthermore, the observation that circHECW2 expression decreased after a two-week treatment suggests its potential as a biomarker for predicting the functional outcome of MDD. However, it is essential to validate these findings in larger sample sizes or postmortem cohorts to establish the specific correlation between circHECW2 and MDD definitively.

To date, there have been no reports about the functional link between circHECW2 and m<sup>6</sup>A methylation in MDD. However, accumulating evidence suggests that the dysregulation of RNA m<sup>6</sup>A methylation may play a role in the pathogenesis of MDD<sup>21,22,54</sup>. Notably, several studies have provided valuable insights into the potential involvement of m<sup>6</sup>A-related genes in MDD. Samaan et al.<sup>20</sup> provided compelling evidence indicating

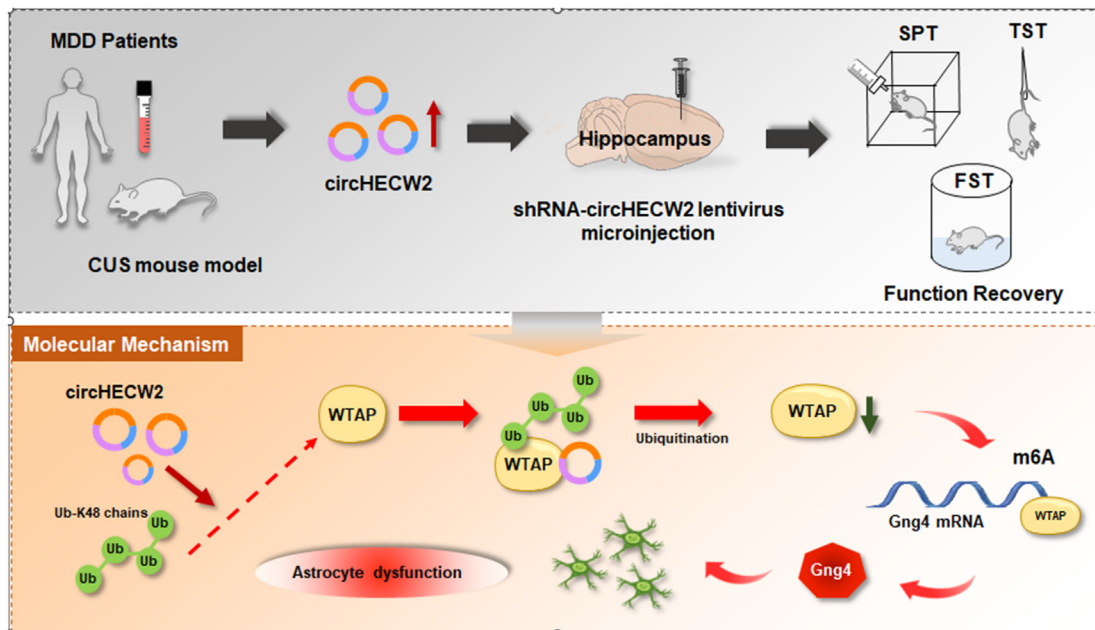


**Figure 8** The circHECW2/WTAP/GNG4 axis regulates astrocyte dysfunction by decreasing GNG4 stability via WTAP-mediated m<sup>6</sup>A modification.

that the FTO rs9939609 A variant may be associated with a decreased risk of depression, independent of its influence on BMI. Du et al.<sup>21</sup> suggested that m<sup>6</sup>A genes may play a role in conferring the risk of MDD. Engel et al.<sup>19</sup> demonstrated that deletion of *Mettl3* or *FTO* in adult neurons alters the m<sup>6</sup>A epi transcriptome, resulting in increased fear memory and changes in the transcriptome response to fear and synaptic plasticity. This suggests that the dysregulation of the m<sup>6</sup>A/m modification in the brain may represent a novel and intricate layer of gene expression regulation following stress, potentially contributing to the pathophysiology of stress-related psychiatric disorders. Given the observed increase in circHECW2 levels in CUS mice, it is hypothesized that certain methylases interact with circHECW2 and downregulate m<sup>6</sup>A levels. One potential candidate is WTAP, which has been suggested to play a role in the development of various clinical symptoms of MDD in the Chinese Han population<sup>21</sup>. WTAP is an essential player in the methyltransferase complex and is involved in many cellular processes<sup>55</sup>. In our studies, we found that circHECW2 can regulate the expression of WTAP but does not alter the levels of other methylases and demethylases in astrocytes. Importantly, Liu et al.<sup>22</sup> demonstrated that WTAP was significantly downregulated in the peripheral blood of MDD patients using microarray analysis and real-time quantitative PCR. This observation aligns to some extent with the results of our study, further supporting the potential involvement of WTAP and m<sup>6</sup>A methylation in MDD.

Data from various sources, including life events, personality disorders, biology, comorbidity, and pharmacology, indicate that depression and anxiety not only share similarities but also exhibit many differences. For example, benzodiazepines are effective for treating anxiety symptoms and most anxiety disorders but do not show significant efficacy in MDD<sup>7</sup>. This suggests that there are differences in the pathological mechanisms of depression and anxiety disorders. Therefore, given the resource limitations and study scope, our research was originally designed to investigate the role of circHECW2 in depression. Additionally, we used the SPT, FST, and TST to assess the anhedonic behavior and feelings of despair in mice. These tests are primarily indicators for evaluating depressive-like behaviors<sup>8</sup>. On the other hand, the open field test (OFT) and elevated plus maze (EPM) are primarily employed to evaluate anxiety-like behaviors by measuring the exploratory tendencies of the animals<sup>8,9</sup>. Given the behavioral tests we used (SPT, FST, and TST), we are currently unable to assess the role of circHECW2 in anxiety. However, antidepressant medications, including selective serotonin reuptake inhibitors, tricyclic antidepressants, and monoamine oxidase inhibitors, are highly effective in the management of comorbid depression and anxiety<sup>10</sup>. Therefore, we hypothesize that circHECW2 may also potentially have a regulatory role in anxiety. However, whether this regulatory effect and mechanism are consistent with its regulation in depression requires further experimental validation.

In the study reported here, we observed that the decreased m<sup>6</sup>A methylation levels of *Gng4* mRNA resulted in the degradation of GNG4 and subsequent astrocyte dysfunction. GNG4 belongs to the G-protein  $\gamma$  subunit family, and it is known to form heterotrimers with the  $\alpha$ - and  $\beta$ -subunits of G proteins. These heterotrimers are involved in transducing signals from upstream G-protein-coupled receptors (GPCRs) to intracellular effectors<sup>56–60</sup>. GNG4 has been reported as a tumor suppressor gene in renal cell carcinoma and glioblastoma<sup>61</sup>. Interestingly, GNG4 exhibits significant expression in key brain regions such as the hippocampus, putamen, and frontal

cortex, and its expression is observed to be decreased in neurodegenerative diseases<sup>62</sup>. Therefore, it is reasonable to speculate that pharmacological interventions aimed at increasing GNG4 levels have the potential to alter the cognitive trajectory in individuals with neurodegenerative diseases. In our study, we found that GNG4 levels were negatively correlated with the scores of the HAMD-cognitive impairment in MDD patients, and further analysis using real resting-state *fMRI* data supported the association between GNG4 and cognitive function in MDD.

In conclusion, we illustrated for the first time that circHECW2 expression level is increased in MDD and positively correlated with HAMD-24, MADRS, and HAMA scores. CircHECW2 may serve as a biomarker for diagnosing and predicting MDD outcomes. Moreover, we found that circHECW2 promotes the ubiquitin-mediated degradation of WTAP, leading to decreased m<sup>6</sup>A methylation levels of *Gng4* mRNA and subsequent degradation of GNG4 in astrocytes, resulting in the attenuation of depressive-like behaviors. Our findings suggest that circHECW2 may be an important and promising target for therapeutic interventions in MDD, providing a new direction for future research in this area.

## 5. Conclusions

We investigated the mechanisms by which these effects are achieved and showed that a central signaling axis, circHECW2/WTAP/GNG4, regulates astrocyte dysfunction in depression. These findings provide new insights into the close relationship between circHECW2 and m<sup>6</sup>A methylation in MDD and demonstrate that circHECW2 may be a potential target for MDD therapy.

## Acknowledgments

This work was supported by grants from the Science and Technology Innovation 2030-Major Project of the Ministry of Science and Technology of China (2021ZD0202904/2021ZD0202900), the National Science Fund Distinguished Young Scholars (82025033, China), the National Natural Science Foundation of China (82230115, 82273914, 81903591, 82372024, 82003733), the Natural Science Foundation of Jiangsu Province (BK20200358, China), ZhiShan Scholar Program of Southeast University (2242022R40059 and 2242021R40023, China), the Jiangsu Provincial Key Laboratory of Critical Care Medicine (JSKLCCM-2022-02-008, China) and the Open Project Program of the Key Laboratory of Developmental Genes and Human Diseases of the Ministry of Education (LDGHD202304, China).

## Author contributions

Honghong Yao, Bing Han, and Ying Bai planned and designed the research. Ying Bai wrote the manuscript. Ying Bai, Han Li, Xue Liu, Daxing Li, Xiaofei Guo, and Xinchun Huo performed the CUS model, behavior test, and Western blot; Ying Bai and Biling Chen performed the Immunostaining. Ying Bai and Hui Ren performed the flow cytometry sorting. Bing Han designed the primers. Ying Bai and Yu Wang performed the 3D reconstruction. Biling Chen, Ying Bai and Han Li performed the LV microinjection. Ying Bai and Biling Chen performed the real time RT-PCR. Minzi Ju, Hui Ren, Di Chang, Mengze Tong and Ying Tan recruited MDD patients and collected of clinical patient blood samples. Di Chang and Ying Bai performed the analysis of clinical samples.

## Conflicts of interest

The authors state that there are no conflicts of interest involved.

## Appendix A. Supporting information

Supporting data to this article can be found online at <https://doi.org/10.1016/j.apsb.2024.01.011>.

## References

- Kennis M, Gerritsen L, van Dalen M, Williams A, Cuijpers P, Bockting C. Prospective biomarkers of major depressive disorder: a systematic review and meta-analysis. *Mol Psychiatr* 2020;**25**:321–38.
- Moussavi S, Chatterji S, Verdes E, Tandon A, Patel V, Ustun B. Depression, chronic diseases, and decrements in health: results from the World Health Surveys. *Lancet* 2007;**370**:851–8.
- Mueller TI, Leon AC, Keller MB, Solomon DA, Endicott J, Coryell W, et al. Recurrence after recovery from major depressive disorder during 15 years of observational follow-up. *Am J Psychiatr* 1999;**156**:1000–6.
- Zhang ZW, Gao CS, Zhang H, Yang J, Wang YP, Pan LB, et al. *Morinda officinalis* oligosaccharides increase serotonin in the brain and ameliorate depression via promoting 5-hydroxytryptophan production in the gut microbiota. *Acta Pharm Sin B* 2022;**12**:3298–312.
- Battle DE. Diagnostic and statistical manual of mental disorders (DSM). *Coda* 2013;**25**:191–2.
- Knight MJ, Baune BT. Cognitive dysfunction in major depressive disorder. *Curr Opin Psychiatr* 2018;**31**:26–31.
- Huang R, Zhang Y, Bai Y, Han B, Ju M, Chen B, et al. N<sup>6</sup>-Methyladenosine modification of fatty acid amide hydrolase messenger RNA in circular RNA STAG1-regulated astrocyte dysfunction and depressive-like behaviors. *Biol Psychiatr* 2020;**88**:392–404.
- Papakostas GI, Ionescu DF. Towards new mechanisms: an update on therapeutics for treatment-resistant major depressive disorder. *Mol Psychiatr* 2015;**20**:1142–50.
- Cipriani A, Furukawa TA, Salanti G, Chaimani A, Atkinson LZ, Ogawa Y, et al. Comparative efficacy and acceptability of 21 antidepressant drugs for the acute treatment of adults with major depressive disorder: a systematic review and network meta-analysis. *Lancet* 2018;**391**:1357–66.
- Undurraga J, Baldessarini RJ. Randomized, placebo-controlled trials of antidepressants for acute major depression: thirty-year meta-analytic review. *Neuropsychopharmacology* 2012;**37**:851–64.
- Kang SG, Cho SE. Neuroimaging biomarkers for predicting treatment response and recurrence of major depressive disorder. *Int J Mol Sci* 2020;**21**:2148.
- Niu Y, Zhao X, Wu YS, Li MM, Wang XJ, Yang YG. N<sup>6</sup>-Methyladenosine (m<sup>6</sup>A) in RNA: an old modification with a novel epigenetic function. *Dev Reprod Biol* 2013;**11**:8–17.
- Shen D, Wang B, Gao Y, Zhao L, Bi Y, Zhang J, et al. Detailed resume of RNA m<sup>6</sup>A demethylases. *Acta Pharm Sin B* 2022;**12**:2193–205.
- Patil DP, Pickering BF, Jaffrey SR. Reading m<sup>6</sup>A in the transcriptome: m<sup>6</sup>A-binding proteins. *Trends Cell Biol* 2018;**28**:113–27.
- Chen M, Wong CM. The emerging roles of N<sup>6</sup>-methyladenosine (m<sup>6</sup>A) deregulation in liver carcinogenesis. *Mol Cancer* 2020;**19**:44.
- Song P, Tayier S, Cai Z, Jia G. RNA methylation in mammalian development and cancer. *Cell Biol Toxicol* 2021;**37**:811–31.
- Wen J, Lv R, Ma H, Shen H, He C, Wang J, et al. Zc3h13 regulates nuclear RNA m<sup>6</sup>A methylation and mouse embryonic stem cell self-renewal. *Mol Cell* 2018;**69**:1028–1038.e6.
- Wang X, Wu R, Liu Y, Zhao Y, Bi Z, Yao Y, et al. m<sup>6</sup>A mRNA methylation controls autophagy and adipogenesis by targeting Atg5 and Atg7. *Autophagy* 2020;**16**:1221–35.
- Engel M, Eggert C, Kaplick PM, Eder M, Roh S, Tietze L, et al. The role of m<sup>6</sup>A/m-RNA methylation in stress response regulation. *Neuron* 2018;**99**:389–403.e9.
- Samaan Z, Anand SS, Zhang X, Desai D, Rivera M, Pare G, et al. The protective effect of the obesity-associated rs9939609 A variant in fat mass- and obesity-associated gene on depression. *Mol Psychiatr* 2013;**18**:1281–6.
- Du T, Rao S, Wu L, Ye N, Liu Z, Hu H, et al. An association study of the m<sup>6</sup>A genes with major depressive disorder in Chinese Han population. *J Affect Disord* 2015;**183**:279–86.
- Liu S, Xiu J, Zhu C, Meng K, Li C, Han R, et al. Fat mass and obesity-associated protein regulates RNA methylation associated with depression-like behavior in mice. *Nat Commun* 2021;**12**:6937.
- Lei M, Zheng G, Ning Q, Zheng J, Dong D. Translation and functional roles of circular RNAs in human cancer. *Mol Cancer* 2020;**19**:30.
- Mehta SL, Dempsey RJ, Vemuganti R. Role of circular RNAs in brain development and CNS diseases. *Prog Neurobiol* 2020;**186**:101746.
- Bai Y, Zhang Y, Han B, Yang L, Chen X, Huang R, et al. Circular RNA DLGAP4 ameliorates ischemic stroke outcomes by targeting miR-143 to regulate endothelial–mesenchymal transition associated with blood–brain barrier integrity. *J Neurosci* 2018;**38**:32–50.
- Zhang Y, Du L, Bai Y, Han B, He C, Gong L, et al. CircDYM ameliorates depressive-like behavior by targeting miR-9 to regulate microglial activation via HSP90 ubiquitination. *Mol Psychiatr* 2020;**25**:1175–90.
- Xu J, Ji L, Liang Y, Wan Z, Zheng W, Song X, et al. CircRNA-SORE mediates sorafenib resistance in hepatocellular carcinoma by stabilizing YBX1. *Signal Transduct Targeted Ther* 2020;**5**:298.
- Yu X, Bai Y, Han B, Ju M, Tang T, Shen L, et al. Extracellular vesicle-mediated delivery of circDYM alleviates CUS-induced depressive-like behaviours. *J Extracell Vesicles* 2022;**11**:e12185.
- Shi Y, Song R, Wang Z, Zhang H, Zhu J, Yue Y, et al. Potential clinical value of circular RNAs as peripheral biomarkers for the diagnosis and treatment of major depressive disorder. *EBioMedicine* 2021;**66**:103337.
- Yang L, Han B, Zhang Y, Bai Y, Chao J, Hu G, et al. Engagement of circular RNA HECW2 in the nonautophagic role of ATG5 implicated in the endothelial-mesenchymal transition. *Autophagy* 2018;**14**:404–18.
- Freeman MR. Specification and morphogenesis of astrocytes. *Science* 2010;**330**:774–8.
- Linnerbauer M, Wheeler MA, Quintana FJ. Astrocyte crosstalk in CNS inflammation. *Neuron* 2020;**108**:608–22.
- Tang Y, Zhou M, Huang R, Shen L, Yang L, Zhou Z, et al. Involvement of HECTD1 in LPS-induced astrocyte activation via sigma-IR–JNK/p38–FOXJ2 axis. *Cell Biosci* 2021;**11**:62.
- Zhang Q, Sun Y, He Z, Xu Y, Li X, Ding J, et al. Kynurenine regulates NLRP2 inflammasome in astrocytes and its implications in depression. *Brain Behav Immun* 2020;**88**:471–81.
- Chen J, Tan Z, Zeng L, Zhang X, He Y, Gao W, et al. Heterosynaptic long-term depression mediated by ATP released from astrocytes. *Glia* 2013;**61**:178–91.
- Serrano A, Haddjeri N, Lacaille JC, Robitaille R. GABAergic network activation of glial cells underlies hippocampal heterosynaptic depression. *J Neurosci* 2006;**26**:5370–82.
- Pascual O, Casper KB, Kubera C, Zhang J, Revilla-Sanchez R, Sul JY, et al. Astrocytic purinergic signaling coordinates synaptic networks. *Science* 2005;**310**:113–6.
- Durkee C, Kofuji P, Navarrete M, Araque A. Astrocyte and neuron cooperation in long-term depression. *Trends Neurosci* 2021;**44**:837–48.
- Wang Q, Jie W, Liu JH, Yang JM, Gao TM. An astroglial basis of major depressive disorder? An overview. *Glia* 2017;**65**:1227–50.
- Zhang Y, Shen K, Bai Y, Lv X, Huang R, Zhang W, et al. Mir143-BBC3 cascade reduces microglial survival via interplay between apoptosis and autophagy: implications for methamphetamine-mediated neurotoxicity. *Autophagy* 2016;**12**:1538–59.

41. Willner P, Towell A, Sampson D, Sophokleous S, Muscat R. Reduction of sucrose preference by chronic unpredictable mild stress, and its restoration by a tricyclic antidepressant. *Psychopharmacology* 1987; **93**:358–64.
42. Xiao Y, Jin J, Chang M, Chang JH, Hu H, Zhou X, et al. Peli1 promotes microglia-mediated CNS inflammation by regulating Traf3 degradation. *Nat Med* 2013; **19**:595–602.
43. Kantzer CG, Boutin C, Herzig ID, Wittwer C, Reiss S, Tiveron MC, et al. Anti-ACSA-2 defines a novel monoclonal antibody for prospective isolation of living neonatal and adult astrocytes. *Glia* 2017; **65**:990–1004.
44. Li S, Nie EH, Yin Y, Benowitz LI, Tung S, Vinters HV, et al. GDF10 is a signal for axonal sprouting and functional recovery after stroke. *Nat Neurosci* 2015; **18**:1737–45.
45. Crouch EE, Doetsch F. FACS isolation of endothelial cells and pericytes from mouse brain microregions. *Nat Protoc* 2018; **13**:738–51.
46. Zhang Y, Zhang Y, Bai Y, Chao J, Hu G, Chen X, et al. Involvement of PUMA in pericyte migration induced by methamphetamine. *Exp Cell Res* 2017; **356**:28–39.
47. Yao H, Ma R, Yang L, Hu G, Chen X, Duan M, et al. MiR-9 promotes microglial activation by targeting MCP1. *Nat Commun* 2014; **5**:4386.
48. Lu CQ, Jiao Y, Meng XP, Cai Y, Luan Y, Xu XM, et al. Structural change of thalamus in cirrhotic patients with or without minimal hepatic encephalopathy and the relationship between thalamus volume and clinical indexes related to cirrhosis. *Neuroimage Clin* 2018; **20**:800–7.
49. Xu XM, Jiao Y, Tang TY, Zhang J, Lu CQ, Luan Y, et al. Dissociation between cerebellar and cerebral neural activities in humans with long-term bilateral sensorineural hearing loss. *Neural Plast* 2019; **2019**:8354849.
50. Li W, Ali T, He K, Liu Z, Shah FA, Ren Q, et al. Ibrutinib alleviates LPS-induced neuroinflammation and synaptic defects in a mouse model of depression. *Brain Behav Immun* 2021; **92**:10–24.
51. Rimmerman N, Verdiger H, Goldenberg H, Naggan L, Robinson E, Kozela E, et al. Microglia and their LAG3 checkpoint underlie the antidepressant and neurogenesis-enhancing effects of electroconvulsive stimulation. *Mol Psychiatr* 2022; **27**:1120–35.
52. Wohleb ES, Terwilliger R, Duman CH, Duman RS. Stress-induced neuronal colony stimulating factor 1 provokes microglia-mediated neuronal remodeling and depressive-like behavior. *Biol Psychiatr* 2018; **83**:38–49.
53. Han X, Xu T, Fang Q, Zhang H, Yue L, Hu G, et al. Quercetin hinders microglial activation to alleviate neurotoxicity via the interplay between NLRP3 inflammasome and mitophagy. *Redox Biol* 2021; **44**:102010.
54. Barbon A, Magri C. RNA editing and modifications in mood disorders. *Genes* 2020; **11**:872.
55. Chen Y, Peng C, Chen J, Chen D, Yang B, He B, et al. WTAP facilitates progression of hepatocellular carcinoma via m6A-HuR-dependent epigenetic silencing of ETS1. *Mol Cancer* 2019; **18**:127.
56. Tanaka H, Kanda M, Miwa T, Umeda S, Sawaki K, Tanaka C, et al. G-protein subunit gamma-4 expression has potential for detection, prediction and therapeutic targeting in liver metastasis of gastric cancer. *Br J Cancer* 2021; **125**:220–8.
57. Garcia-Regalado A, Guzman-Hernandez ML, Ramirez-Rangel I, Robles-Molina E, Balla T, Vazquez-Prado J, et al. G protein-coupled receptor-promoted trafficking of Gβ1γ2 leads to AKT activation at endosomes via a mechanism mediated by Gβ1γ2–Rab11a interaction. *Mol Biol Cell* 2008; **19**:4188–200.
58. Khan SM, Sleno R, Gora S, Zylbergold P, Laverdure JP, Labbe JC, et al. The expanding roles of Gβγ subunits in G protein-coupled receptor signaling and drug action. *Pharmacol Rev* 2013; **65**:545–77.
59. Crespo P, Xu N, Simonds WF, Gutkind JS. Ras-dependent activation of MAP kinase pathway mediated by G-protein β γ subunits. *Nature* 1994; **369**:418–20.
60. Zhang J, Liu W, Liu J, Xiao W, Liu L, Jiang C, et al. G-protein β2 subunit interacts with mitofusin 1 to regulate mitochondrial fusion. *Nat Commun* 2010; **1**:101.
61. Pal J, Patil V, Mondal B, Shukla S, Hegde AS, Arivazhagan A, et al. Epigenetically silenced GNG4 inhibits SDF1α/CXCR4 signaling in mesenchymal glioblastoma. *Genes Cancer* 2016; **7**:136–47.
62. Bonham LW, Evans DS, Liu Y, Cummings SR, Yaffe K, Yokoyama JS. Neurotransmitter pathway genes in cognitive decline during aging: evidence for GNG4 and KCNQ2 genes. *Am J Alzheimers Dis Other Demen* 2018; **33**:153–65.